Quantum free-energy differences from nonequilibrium path integrals. II. Convergence properties for the harmonic oscillator

Ramses van Zon,[1] Lisandro Hernández de la Peña,[2,3] Gilles H. Peslherbe,[3] and Jeremy Schofield[1]
[1]*Chemical Physics Theory Group, Department of Chemistry, University of Toronto, 80 Saint George Street, Toronto, Ontario, Canada M5S 3H6*
[2]*Department of Chemistry, University of Illinois at Urbana-Champaign, Urbana, Illinois 61801, USA*
[3]*Centre for Research in Molecular Modeling and Department of Chemistry and Biochemistry, Concordia University, 7141 Sherbrooke Street West, Montréal, Québec, Canada H4B 1R6*
(Received 4 July 2008; published 2 October 2008)

Nonequilibrium path-integral methods for computing quantum free-energy differences are applied to a quantum particle trapped in a harmonic well of uniformly changing strength with the purpose of establishing the convergence properties of the work distribution and free energy as the number of degrees of freedom M in the regularized path integrals goes to infinity. The work distribution is found to converge when M tends to infinity regardless of the switching speed, leading to finite results for the free-energy difference when the Jarzynski nonequilibrium work relation or the Crooks fluctuation relation are used. The nature of the convergence depends on the regularization method. For the Fourier method, the convergence of the free-energy difference and work distribution go as $1/M$, while both quantities converge as $1/M^2$ when the bead regularization procedure is used. The implications of these results to more general systems are discussed.

DOI: 10.1103/PhysRevE.78.041104 PACS number(s): 05.30.−d, 05.70.Ln

I. INTRODUCTION

In the preceding paper [1], a nonequilibrium path-integral method for computing free-energy differences based on combining the Jarzynski equality [2,3] and the Crooks fluctuation relation [4,5] with the path-integral formulation of the quantum mechanical partition sum [6–9] was presented. The path-integral representation of the canonical partition function is based on mapping a quantum system at finite temperature onto a classical system with additional degrees of freedom. A nonequilibrium process can be carried out on this isomorphic classical system along a well-defined trajectory in fictitious time. The Jarzynski and Crooks relations are valid for such a process, but only under the assumption that the work distribution converges as the parameter M of the regularization procedure applied to the infinite dimensional path integral goes to infinity.

A regularization procedure is needed because particles are represented as objects with an infinite number of degrees of freedom in the path-integral formulation. As a result, nonequilibrium dynamical processes in this representation can lead to divergences in nonphysical quantities, such as the average total Hamiltonian of the particle or the work performed on the system in the fictitious process, which is a central quantity in the Jarzynski and Crooks relations. A regularization procedure restricts the number of degrees of freedom to a finite number M and results in finite but M-dependent estimators for quantities of interest. In the regularized path-integral representation, one finds that the expression for the work takes the form of the difference between two quantities which diverge as $M\to\infty$. Having an estimator for physical quantities that take the form of the difference between two diverging quantities is not unusual in the context of path integrals [8], but this does make it important to establish the convergence properties of all relevant estimators. Furthermore, even when it can be demonstrated that the regularization procedure leads to convergent results, the viability of the nonequilibrium path-integral method as a means of computing quantum free-energy differences is strongly dependent on the rate of convergence of the regularized path integral to the exact quantum result. Neither the convergence nor the rate of convergence was addressed in detail in Ref. [1], although strong numerical evidence of convergence was presented for a quantum particle in a quartic potential.

In this paper, the rate of convergence of different regularization procedures is examined in detail for the special case of a quantum harmonic oscillator. Harmonic systems have the advantage of being often amenable to analytical treatment, allowing for closed form and exact solutions. Here, the convergence of the regularization procedure is studied in three regimes of the nonequilibrium process, i.e., the quasistatic, the finite time, and instantaneous switching. The work distribution is computed for each of these regimes and its convergence, as well as the convergence of free-energy difference are analyzed as the number of degrees of freedom goes to infinity. It will be shown that the free-energy difference and the work distribution converge for both the Fourier and the bead regularization procedures [1], with the latter converging more quickly.

The paper is organized as follows: Sec. II presents a brief overview of the method as it applies to the harmonic oscillator. Section III contains the analysis of the convergence of the free energy under different regularization schemes. The work distributions will be determined using a generating function technique explained in Sec. IV. In Secs. V–VII the quasistatic, finite time, and instantaneous switching processes, respectively, are studied. A comparison between the nonequilibrium work distribution generated by the fictitious dynamics and that generated with real time quantum dynamics is made in Sec. VIII. The conclusions are given in Sec. IX.

II. METHOD AND MODEL SYSTEM

We consider a one-dimensional quantum system with a Hamiltonian operator $\hat{H}(\lambda)=\hat{T}+\hat{V}$, with $\hat{T}=\hat{p}^2/(2m)$ and $\hat{V}=V(\hat{x},\lambda)=\frac{1}{2}m\lambda\hat{x}^2$. Here the potential energy V depends on a control parameter λ, which is equal to the square of the frequency ω. The canonical partition function of this system at an inverse temperature β is defined by

$$Z(\lambda)=e^{-\beta F(\lambda)}=\mathrm{Tr}\, e^{-\beta\hat{H}(\lambda)}, \tag{1}$$

and can be written as [6,7]

$$Z(\lambda)=\int \mathcal{D}x e^{-(1/\hbar)S[x,\lambda]}, \tag{2}$$

where the integral is over closed paths $x(s)$ [i.e., $x(\beta\hbar)=x(0)$] and the Euclidean action S is a functional of x given by

$$S[x,\lambda]=\int_0^{\beta\hbar} ds\left[\frac{1}{2}m\left(\frac{dx}{ds}\right)^2+\frac{1}{2}m\lambda x^2\right]. \tag{3}$$

Here and below the s dependence of x in integrals over s will always be implied. For this one-dimensional harmonic system, the quantum free energy is known to be exactly

$$F(\lambda)=\beta^{-1}\ln[2\sinh(\beta\hbar\omega/2)]. \tag{4}$$

The nonequilibrium path-integral approach of computing free-energy differences uses a nonequilibrium process defined by a fictitious dynamics in which λ is changed from $\lambda_A=\omega_A^2$ to $\lambda_B=\omega_B^2$ over a time τ, while starting at canonical equilibrium corresponding to $\lambda=\lambda_A$. This fictitious dynamics is derived by introducing a new field $p(s)$ which is also periodic in imaginary time, satisfying $p(s)=p(s+\beta\hbar)$, leading to an expression that has the form of a classical partition function as follows:

$$Z(\lambda)=C\int \mathcal{D}x\mathcal{D}p e^{-\beta H[x,p,\lambda]}, \tag{5}$$

where the fictitious Hamiltonian is given by

$$H[x,p,\lambda]=\int_0^1 du\left[\frac{p^2}{2m}+\frac{1}{2}\kappa\left(\frac{dx}{du}\right)^2+\frac{1}{2}m\lambda x^2\right]. \tag{6}$$

Here $u=s/(\beta\hbar)$ is a scaled imaginary time variable and the string tension is

$$\kappa=\frac{m}{\beta^2\hbar^2}.$$

We are interested in a Hamiltonian process, with equations of motion

$$\frac{\partial x}{\partial t}=\frac{\delta H[x,p,\lambda]}{\delta p(u)}=\frac{p}{m}, \tag{7a}$$

$$\frac{\partial p}{\partial t}=-\frac{\delta H[x,p,\lambda]}{\delta x(u)}=\kappa\frac{\partial^2 x}{\partial u^2}-m\lambda x, \tag{7b}$$

in which λ is time dependent, and satisfies the boundary conditions $\lambda(0)=\lambda_A$ and $\lambda(\tau)=\lambda_B$. Then, defining the fictitious work as

$$W=H[x(\tau),p(\tau),\lambda_B]-H[x,p,\lambda_A], \tag{8}$$

the following identities were shown to hold [1]:

$$\langle e^{-\beta W}\rangle_{\lambda_A}=e^{-\beta\Delta F}, \tag{9}$$

and

$$P_f(W)=e^{\beta W}e^{-\beta\Delta F}P_r(-W), \tag{10}$$

where $\langle\ \rangle_{\lambda_A}$ denotes an average over nonequilibrium trajectories whose initial conditions are drawn from a canonical distribution with $\lambda=\lambda_A$, $\Delta F=F(\lambda_B)-F(\lambda_A)$, $P_f(W)$ is the probability density to do an amount of work W during the process that takes λ from λ_A to λ_B (the *forward* process), and $P_r(-W)$ is the probability density to do work $-W$ during a similar process that starts at λ_B and ends at λ_A (the *reverse* process). Equations (9) and (10) are the Jarzynski's nonequilibrium work relation and Crooks fluctuation relation, respectively.

The distribution of the work done as a result of the change in ω will be studied for this model. This distribution can be used either in the Jarzynski relation (9) or in the Crooks fluctuation relation (10) to determine the free-energy difference, both of which should yield $\Delta F=F_B-F_A=\beta^{-1}\ln[\sinh(\beta\hbar\omega_B/2)/\sinh(\beta\hbar\omega_A/2)]$.

The work in Eq. (8) is expressed as the difference of the fictitious Hamiltonian at two times. The average value of the fictitious Hamiltonian diverges in canonical equilibrium due to the infinite number of degrees of freedom in the path integral (2), which might pose a problem for the very definition of the work distributions. To investigate whether the work distribution is well defined, it is necessary to limit the system to a finite number of degrees of freedom. In Ref. [1], two different regularization methods of reducing the path-integral representations to a finite number of dimensions were introduced. While both schemes are similar in their Fourier representations, in one case the degrees of freedom correspond to low-frequency modes of the continuous closed string, whereas in the other case they represent a discretized lattice version of the string. In the first case the regularization is based on statistical arguments motivated by the form of the resulting Hamiltonian, and in the second case the regularization is introduced in the lattice representation by means of the Trotter formula.

For finite M, the value of ΔF found using the work distribution differs from the exact quantum result. In fact, for the harmonic oscillator, one can express the free energy explicitly as an expansion in inverse powers of M, and thus assess the convergence of ΔF analytically. This will be studied first in Sec. III, in which alternative regularizations aimed at improving the convergence are also discussed. Note that the convergence of the free energy only requires equilibrium considerations. Then, in Secs. V–VII, the convergence of the nonequilibrium work distributions is analyzed for the cases

of an infinitely slow switching rate, a finite switching rate, and an instantaneous switching process, respectively.

III. FREE ENERGY UNDER DIFFERENT REGULARIZATIONS

Analytical considerations of the harmonic system proceed most easily in the Fourier representation. As explained in Ref. [1], the Fourier transformation takes on slightly different forms in the Fourier and the bead regularization methods. In both cases, though, the Hamiltonian assumes the form

$$H = \sum_{|k|\leq k_c} H_k, \tag{11}$$

where k_c is a cutoff wave vector, and

$$H_k = \frac{|\tilde{p}_k|^2}{2m} + \frac{1}{2}m\Omega_k^2|\tilde{x}_k|^2, \tag{12}$$

with

$$\Omega_k^2 = \omega_k^2 + \omega^2. \tag{13}$$

The dispersion relation for the Fourier regularization is given by

$$\omega_k = 2\pi k\sqrt{\frac{\kappa}{m}} = \frac{2\pi k}{\hbar\beta}, \tag{14}$$

while that for the bead regularization is

$$\omega_k = \frac{2M}{\hbar\beta}\sin\frac{\pi k}{M}. \tag{15}$$

Note that in the Fourier regularization, k_c is a chosen cutoff, whereas from the Fourier transform of the bead regularization, we have $k_c=\lfloor(M-1)/2\rfloor$ or, for M odd, $M=2k_c+1$. Thus, the two regularization methods can be parametrized either by k_c or M.

Given the Hamiltonian in Eq. (12), the partition sum may be written as

$$Z_M(\lambda) = C\prod_{|k|\leq k_c}\int d\tilde{p}_k d\tilde{x}_k e^{-\beta H_k}, \tag{16}$$

where C is independent of λ. Each integral is Gaussian and can be explicitly evaluated. Since each mode occurs twice in the product (as k and $-k$) except for $k=0$, one finds for $e^{-\beta\Delta F}$,

$$e^{-\beta\Delta F} = \lim_{M\to\infty}\frac{Z_M(\lambda_B)}{Z_M(\lambda_A)} = \lim_{k_c\to\infty}\frac{\omega_A}{\omega_B}\prod_{k=1}^{k_c}\frac{\omega_k^2+\omega_A^2}{\omega_k^2+\omega_B^2}. \tag{17}$$

This product must be evaluated separately for the two different dispersion relations of the Fourier and the bead regularization schemes in Eqs. (14) and (15), respectively.

In the Fourier regularization with the dispersion relation given by Eq. (14), Eq. (17) can be evaluated in the limit $k_c\to\infty$ by writing

$$e^{-\beta\Delta F} = \frac{\omega_A}{\omega_B}\prod_{k=1}^{\infty}\left[1+\left(\frac{\beta\hbar\omega_A}{2\pi k}\right)^2\right]\prod_{k'=1}^{\infty}\left[1+\left(\frac{\beta\hbar\omega_B}{2\pi k'}\right)^2\right]^{-1}, \tag{18}$$

and using the identity [10]

$$\frac{\sinh z}{z} = \prod_{k=1}^{\infty}\left(1+\frac{z^2}{k^2\pi^2}\right),$$

to finally obtain the exact quantum result

$$e^{-\beta\Delta F} = \frac{\sinh(\beta\hbar\omega_A/2)}{\sinh(\beta\hbar\omega_B/2)}. \tag{19}$$

It is straightforward to show using Eq. (17) that the limit is approached as $k_c^{-1}=\mathcal{O}(M^{-1})$.

For the bead regularization, on the other hand, one uses Eq. (15) and $M=2k_c+1$ to write Eq. (17) as

$$e^{-\beta\Delta F} = \lim_{M\to\infty}\left[\prod_{k=1}^{M}\frac{\sin^2\frac{\pi k}{M}+\left(\frac{\hbar\beta\omega_A}{2M}\right)^2}{\sin^2\frac{\pi k}{M}+\left(\frac{\hbar\beta\omega_B}{2M}\right)^2}\right]^{1/2} = \lim_{M\to\infty}\left[\prod_{k=1}^{M}\frac{2+\left(\frac{\hbar\beta\omega_A}{M}\right)^2-2\cos\frac{2\pi k}{M}}{2+\left(\frac{\hbar\beta\omega_B}{M}\right)^2-2\cos\frac{2\pi k}{M}}\right]^{1/2}. \tag{20}$$

One then uses a different identity, namely [11],

$$\frac{1}{2}\prod_{k=1}^{M}\left(z-2\cos\frac{2\pi k}{M}\right) = \cosh\left(M\,\mathrm{arccosh}\,\frac{z}{2}\right)-1, \tag{21}$$

to arrive at

$$e^{-\beta\Delta F} = \lim_{M\to\infty}\left[\frac{\cosh\left\{M\,\mathrm{arccosh}\left[1+\frac{1}{2}\left(\frac{\hbar\beta\omega_A}{M}\right)^2\right]\right\}-1}{\cosh\left\{M\,\mathrm{arccosh}\left[1+\frac{1}{2}\left(\frac{\hbar\beta\omega_B}{M}\right)^2\right]\right\}-1}\right]^{1/2}, \tag{22}$$

which reduces to Eq. (19) as well when the limit $M\to\infty$ is evaluated, with correction terms of order M^{-2} (see, e.g., Ref. [11]).

There are other regularization methods possible which lead to even faster convergence of the free energy at the expense of a more complicated regularized Hamiltonian. Such higher-order schemes can be derived systematically by exploiting the analogy between the bead representation and the Hamiltonian-splitting method used to obtain integrators in molecular dynamics. In fact, the basis of the bead regularization is the splitting form in Eq. (30) of the preceding paper [1], and that same form is also the basis of the Verlet scheme to integrate the equations of motion for classical Hamiltonian systems in molecular dynamics simulations [12]. The advantage of using splitting schemes to derive integrators for molecular dynamics is that the approximate dy-

namics is still symplectic, causing such integration schemes to be very stable. The analogous property to symplecticity in the path-integral context is the Hermitian nature of the Boltzmann operator, which is preserved in splitting schemes.

In an attempt to reduce the error due to operator splitting, many alternative splitting schemes for molecular dynamics simulations have been derived (see Ref. [13], and references therein). Some of these schemes raise the order of the splitting approximation to $\mathcal{O}(\delta t^4)$ or higher. Such splitting schemes can also be used for path integrals and result in a fictitious Hamiltonian in which the beads are not all equivalent or which contains explicit correction terms of order $\mathcal{O}(\hbar^2)$ in the potential, and whose partition function converges to the real quantum partition sum as $\mathcal{O}(M^{-4})$ or higher. Other splitting schemes derived for molecular dynamics simulations are aimed at reducing the error by minimizing the prefactors in front of the leading correction terms [14]. These methods, however, are based on the assumption that different correction terms contribute independently and equally to the error. This approach has proved useful in molecular dynamics simulations. For instance, it has been demonstrated that an optimized second-order scheme called HOA2 can often outperform the Verlet scheme in molecular dynamics simulations of rigid water molecules [15].

We will briefly consider the HOA2 operator-splitting scheme applied as a means to regularize imaginary-time path integrals, since it is the simplest splitting method that may improve the rate of convergence of the regularization. It is based on the following operator-splitting scheme:

$$e^{-\beta\hat{H}/M} = e^{-\eta\beta\hat{V}/M}e^{-\beta\hat{T}/(2M)}e^{-(1-2\eta)\beta\hat{V}/(2M)}e^{-\beta\hat{T}/(2M)}e^{-\eta\beta\hat{V}/M} + \mathcal{O}(M^{-3}). \tag{23}$$

For $\eta=1/4$, this splitting scheme reduces to the path-integral analog of the Verlet scheme of molecular dynamics (applied twice), which corresponds to the standard bead regularization procedure. However, taking a different value of η, namely, $\eta=0.193\,183\,327\,503\,783\,6$, minimizes the sum of the squares of the error terms of $\mathcal{O}(M^{-3})$ [14]. It is shown in Appendix A that when applied to the dynamics of a classical harmonic oscillator, this scheme conserves energy better than the Verlet scheme. The application of the HOA2 splitting scheme to path integrals is carried out by representing the Boltzmann operator by M factors of $\exp(-\beta\hat{H}/M)$, taking its trace to get the partition function, using the splitting scheme (23) for each factor, inserting completeness relations between each exponential, and performing the momentum integration. This procedure leads to a regularized path integral with Hamiltonian

$$H_M = \sum_{n=1}^{M}\left\{\frac{mM}{\hbar^2\beta^2}[(v_n-u_n)^2+(u_{n+1}-v_n)^2] + \frac{1}{2M}[w_1U(u_n)+w_2U(v_n)]\right\}. \tag{24}$$

Here, $w_1=4\eta$, $w_2=2-4\eta$ and the u_n and v_n are the positions of the odd and the even beads, respectively. Odd and even beads are no longer identical in nature when $\eta\neq 1/4$ because

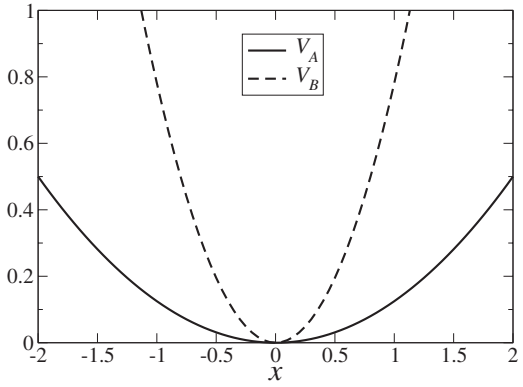

FIG. 1. The two harmonic potentials $\frac{1}{2}m\omega^2x^2$ for which the free-energy difference and the work distribution in switching from one to the other is studied. In both cases, $m=1$, while for V_A, $\omega=\omega_A=1/2$ and for V_B, $\omega=\omega_B=5/4$.

the completeness relation inserted either in front of the $e^{-(1-2\eta)\beta\hat{V}/(2M)}$ or the $e^{-\eta\beta\hat{V}/M}$ in Eq. (23) gives rise to different potential strengths w_2 and w_1. The partition sum $Z_M=\int d^Mu d^Mv\,\exp(-\beta H_M)$ is of Gaussian form, since H_M can be written as $H_M=\Gamma^T\mathsf{V}\Gamma$, with $\Gamma=(u_1,v_1,u_2,v_2,\ldots)$. The integral can be evaluated in terms of the determinant of the matrix V. For the Verlet-type Hamiltonian, a Fourier transform could be used to diagonalize the matrix (i.e., to decouple the modes), which facilitates the determination of the eigenvalues and thus the determinant of V. Here, a Fourier transform only yields a partial diagonalization, i.e., defining

$$\begin{pmatrix}\tilde{u}_k\\ \tilde{v}_k\end{pmatrix} = \frac{1}{\sqrt{2}M}\sum_{n=1}^{M}e^{-2\pi ikn/M}\begin{pmatrix}u_n\\ e^{-\pi ik/M}v_n\end{pmatrix} \tag{25}$$

(where the factor $\sqrt{2}$ and the shift in the phase in front of v_n are introduced for convenience), one gets

$$H_M = \sum_{k=1}^{M}(\tilde{u}_k^* \quad \tilde{v}_k^*)\mathsf{W}_k\begin{pmatrix}\tilde{u}_k\\ \tilde{v}_k\end{pmatrix}, \tag{26}$$

with

$$\mathsf{W}_k = \frac{4M^2}{\beta^2\hbar^2}\begin{pmatrix}2+w_1\left(\frac{\beta\hbar\omega}{2M}\right)^2 & -2\cos\frac{\pi k}{M}\\ -2\cos\frac{\pi k}{M} & 2+w_2\left(\frac{\beta\hbar\omega}{2M}\right)^2\end{pmatrix}.$$

Since each term in the Hamiltonian is simply a 2×2 quadratic form, the partition sum can be written as a product of two-dimensional Gaussian integrals, each of which is proportional to $1/\sqrt{\det\mathsf{W}_k}$. The finite-$M$ partition sum thus becomes

$$Z_M = \prod_{k=1}^{M}\frac{1}{\left[2+4\left(\frac{\beta\hbar\omega}{2M}\right)^2+w_1w_2\left(\frac{\beta\hbar\omega}{2M}\right)^4-2\cos\frac{2\pi k}{M}\right]^{1/2}}. \tag{27}$$

Using the identity in Eq. (21) gives the result

$$Z_M = \frac{1}{\sqrt{2\left[\cosh\left\{M \operatorname{arccosh}\left[1+\frac{1}{2}\left(\frac{\beta\hbar\omega}{M}\right)^2+\frac{w_1 w_2}{32}\left(\frac{\beta\hbar\omega}{M}\right)^4\right]\right\}-1\right]}}. \tag{28}$$

By expanding Z_M in M, one can write this as

$$Z_M = \frac{1}{2\sinh(\beta\hbar\omega/2)}\left[1+\frac{z(\eta)(\beta\hbar\omega/2)^3}{\tanh(\beta\hbar\omega/2)M^2}+O(M^{-4})\right],$$

where the prefactor for the first correction term is $z(\eta)=1/6-\eta+2\eta^2$. Thus, different values of η lead to different convergence properties since $z(\eta)$ depends explicitly on η. The leading order correction is minimized by choosing $z(\eta)=0$, i.e., $\eta=1/4$, which corresponds to the standard bead regularization procedure. Other choices for η lead to larger correction terms and hence slower convergence.

We therefore conclude that using a different splitting scheme can be useful for path integrals if the order of the approximation is changed, but that optimized splitting methods need not yield any improvement, even if they have been shown to be beneficial in the context of molecular dynamics simulations. We will therefore work only with the Verlet-type Hamiltonian in the remainder of this paper.

IV. GENERATING FUNCTION OF THE WORK DISTRIBUTION

The calculation of the work distribution proceeds most easily by first determining its generating function (which coincides with its Fourier transform)

$$G(u) = \int_{-\infty}^{\infty} dW e^{iuW} P(W) \tag{29}$$

$$= \langle e^{iu[H(\tau)-H(0)]}\rangle_{\omega_A}, \tag{30}$$

where $H(t)=H(\tilde{\mathbf{x}}(t),\tilde{\mathbf{p}}(t),\lambda(t))$, which in this case can be written as in Eq. (11).

The equations of motion are given by

$$\frac{d\tilde{x}_k}{dt} = \frac{\tilde{p}_k}{m}, \tag{31a}$$

$$\frac{d\tilde{p}_k}{dt} = -m\Omega_k^2(t)\tilde{x}_k. \tag{31b}$$

From the equations of motion, it is apparent that all Fourier modes evolve independently with a time-dependent frequency, and that each mode contributes an independent term

$$W_k = H_k(\tau) - H_k(0) \tag{32}$$

to the total work $W=\Sigma_{|k|\leq k_c} W_k$. Furthermore, the modes are also independent in the initial canonical distribution function $\exp[-\beta H(\tilde{\mathbf{x}},\tilde{\mathbf{p}},\omega_A^2)]$. Because the generating function of the sum of independent term is the product of the generating functions of the different terms, we get for $G(u)$

$$G(u) = \prod_{|k|\leq k_c} G_k(u), \tag{33}$$

where

$$G_k(u) = \frac{\int dx_k dp_k e^{iuW_k-\beta H_k(0)}}{\int dx_k dp_k e^{-\beta H_k(0)}}. \tag{34}$$

Below, we will investigate the convergence of the work distribution functions P_f and P_r as M is taken to infinity.

V. QUASISTATIC PROCESS

A. Work distribution

Consider first a process in which ω is changed infinitely slowly or quasistatically from ω_A to ω_B. Since each mode k is equivalent to a classical harmonic oscillator with frequency Ω_k, and Ω_k changes from $\Omega_k(0)=\sqrt{\omega_k^2+\omega_A^2}$ to $\Omega_k(\tau)=\sqrt{\omega_k^2+\omega_B^2}$, one can use that $H_k(t)/\Omega_k(t)$ is an adiabatic invariant for harmonic oscillators [16], to obtain for the work

$$W_k = [\Omega_k(\tau)/\Omega_k(0)-1]H_k(0). \tag{35}$$

Equation (34) then gives for the generating functions of mode k,

$$G_k(u) = \frac{1}{1-iu/\gamma_k}, \tag{36}$$

where

$$\gamma_k = \beta\left[\sqrt{\frac{\omega_k^2+\omega_B^2}{\omega_k^2+\omega_A^2}}-1\right]^{-1}. \tag{37}$$

Note that all γ_k have the same sign as $\omega_B-\omega_A$, cf. Eq. (37). The inverse Fourier transform of Eq. (36) is

$$P_k(W) = |\gamma_k| e^{-\gamma_k W}\Theta(\gamma_k W), \tag{38}$$

where Θ is the Heaviside step function. The inverse Fourier transform of $G(u)$ in Eq. (33) is a convolution of these exponential functions, which yields

$$P(W) = \Theta(\gamma_0 W)\sum_{k=0}^{k_c}\Gamma_k(W)e^{-\gamma_k W}, \tag{39}$$

where the form of $\Gamma_k(W)$ depends on whether mode k is degenerate or not. For degenerate modes with $\gamma_k=\gamma_{-k}$ (i.e., $1\leq k\leq\lfloor\frac{M-1}{2}\rfloor$), $\Gamma_k(W)$ is a linear function of W,

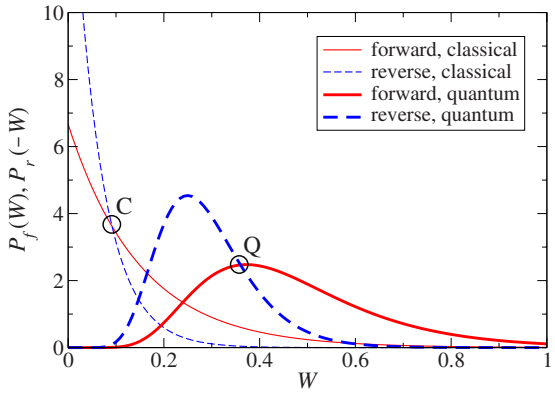

FIG. 2. (Color online) Classical and quantum forward (P_f) and reverse (P_r) work distributions for a quasistatic switching between the potentials in Fig. 1, generated from Eq. (39) using the bead dispersion relation (15), with $M=0$ (classical case) and $M=15$ (quantum case, converged up to $\approx 5\%$). The circles labeled C and Q are the crossing points of the classical and the quantum distributions, respectively, whose W values should coincide with the classical and quantum free-energy differences, according to the Crooks fluctuation relation (10).

$$\Gamma_k(W) = \frac{|\gamma_k|}{\prod_{\substack{|q|\leqslant k_c \\ |q|\neq k}} \left(1 - \frac{\gamma_k}{\gamma_q}\right)} \left(\gamma_k W + \sum_{\substack{|q|\leqslant k_c \\ |q|\neq k}} \frac{1}{1 - \frac{\gamma_q}{\gamma_k}}\right), \quad (40a)$$

while for nondegenerate modes ($k=0$, and $k=\frac{M}{2}$ if M is even), $\Gamma_K(W)$ is a constant given by

$$\Gamma_k(W) = \frac{|\gamma_k|}{\prod_{\substack{|q|\leqslant k_c \\ q\neq k}} \left(1 - \frac{\gamma_k}{\gamma_q}\right)}. \quad (40b)$$

As an example, let the frequency of the harmonic oscillator be switched from $\omega_A=1/2$ to $\omega_B=5/4$, while setting $m=\hbar=1$ and $\beta=10$ (see Fig. 1). In Fig. 2, the forward and reverse work distributions are plotted, using Eq. (39) with $M=0$ and $M=15$, where, for the reverse process, the values of ω_A and ω_B are interchanged. The value of $M=15$ was chosen because the work distribution has then already converged up to about 5%, while $M=0$ corresponds to the classical process. As explained in the preceding paper [1], the work values at crossing points of the forward and reverse distributions should be equal to the free-energy difference. In Fig. 2, the classical distributions are seen to cross at $W_c \approx 0.09$, which agrees with the prediction $\Delta F_{\text{classical}} = \beta^{-1} \ln(\omega_B/\omega_A) = 0.0916\ldots$, while the quantum distributions cross at $W_c \approx 0.36$, which agrees with the prediction $\Delta F_{\text{quantum}} = \beta^{-1} \ln[(\sinh(\hbar\beta\omega_B/2)/\sinh(\hbar\beta\omega_A/2)] = 0.375\ldots$ within 4%. Better agreement for the quantum case is obtained by using higher values of M.

B. Convergence of the work distribution

Although the distribution functions in Fig. 2 suggest a numerical convergence, one can prove analytically that they converge by analyzing the cumulants of the distributions, rather than the somewhat cumbersome infinite products and sums in Eqs. (40a) and (40b). The cumulants κ_j of the distribution $P(W)$ follow from the generating function as

$$\kappa_j = \left[\frac{d}{d(iu)}\right]^j \ln G(u)\Big|_{u=0}, \quad (41)$$

which means the generating function can be expressed in terms of cumulants as

$$\ln G(u) = \sum_{j=1}^{\infty} \frac{\kappa_j}{j!} (iu)^j. \quad (42)$$

The cumulants are therefore also formally related to the free-energy difference by the Jarzynski relation (9), i.e.,

$$\Delta F = -\frac{1}{\beta} \ln\langle e^{-\beta W}\rangle = -\frac{1}{\beta} \ln G(i\beta) = \sum_{j=1}^{\infty} \frac{\kappa_j}{j!} (-\beta)^{j-1}. \quad (43)$$

Cumulants of independent variables are additive, so that

$$\kappa_j = \sum_{|k|\leqslant k_c} \kappa_j^{(k)} = \sum_{|k|\leqslant k_c} \frac{(j-1)!}{\gamma_k^j}, \quad (44)$$

where the mode cumulants were determined from Eq. (36). The convergence of the cumulants as $k_c \to \infty$ can be determined now. From Eq. (37), one sees that

$$\gamma_k \overset{k\gg 1}{\to} \frac{2\beta\omega_k^2}{\Delta\omega^2}, \quad (45)$$

where

$$\Delta\omega^2 = \omega_B^2 - \omega_A^2, \quad (46)$$

and therefore

$$\kappa_j^{(k)} \sim (j-1)! \left(\frac{\Delta\omega^2}{2\beta\omega_k^2}\right)^j. \quad (47)$$

The effect of this asymptotic formula is different in the Fourier and in the bead regularization. In the Fourier regularization, $\omega_k \sim k$, so that $\kappa_j^{(k)} \sim 1/k^{2j}$. Thus one sees that not only do all cumulants in Eq. (44) converge as $k_c \to \infty$, higher-order cumulants converge faster than lower orders, i.e.,

$$\kappa_j(k_c) - \kappa_j(\infty) = \mathcal{O}(1/k_c^{2j-1}) = \mathcal{O}(1/M^{2j-1}). \quad (48)$$

This means that the shape of the work distribution converges faster than the average. However, this property turns out not to be robust. One can show that adding a perturbative quartic term to the potential causes *all* cumulants to converge as k_c^{-1} in the Fourier regularization [17].

The asymptotic convergence of the cumulants is different in the bead regularization scheme, as is evident when the sum in Eq. (44) is first split up into a sum from $k=-k^*$ to k^* and a sum of modes with $k^* \leqslant |k| \leqslant k_c = M/2$, and the latter is approximated by an integral as follows:

$$\kappa_j \sim C_j + 2(j-1)!\left(\frac{\Delta\omega^2}{2\beta}\right)^j \int_{k^*}^{M/2} \frac{dk}{\omega_k^{2j}}, \tag{49}$$

where C_j is the contribution of the $k<k^*$ modes. If $k^*=\mathcal{O}(\hbar\beta\sqrt{\Delta\omega^2})$, C_j can be shown to converge quickly as $M\to\infty$. Using Eq. (15), one gets

$$\frac{\kappa_j - C_j}{2(j-1)!} \sim \left(\frac{\beta\hbar^2\Delta\omega^2}{8M^2}\right)^j M \int_{k^*/M}^{1/2} \frac{dq}{\sin^{2j}(\pi q)}, \tag{50}$$

where the integration variable was changed to $q=k/M$. The integral can be performed using

$$\int^x \frac{dx'}{\sin^{2j} x'} = -\sum_{i=0}^{j-1} \frac{(2j-2)!!(2i-1)!!}{(2j-1)!!(2i)!!} \frac{\cos x}{\sin^{2i+1} x},$$

leading to

$$\frac{\kappa_j - C_j}{2(j-1)!} \sim -\left(\frac{\beta\hbar^2\Delta\omega^2}{8\pi^2}\right)^j \frac{1}{2j-1}\frac{1}{k^{*2j-1}} + \mathcal{O}(M^{-2}). \tag{51}$$

Thus all cumulants in the bead regularization converge as $1/M^2$. Note that this behavior is consistent with the numerical results presented in Fig. 3 of the preceding paper [1].

Even though all cumulants converge in the same way, the coefficients in front of the $1/M^2$ terms often turn out to get smaller for higher-order cumulants, so that the shape will still appear to converge rather quickly, as Fig. 3 illustrates: for large enough M, the shapes of the forward work distributions for different values of M are very similar, but shifted along the W axis.

Since the cumulants of the work distribution converge in the limit $M\to\infty$ in both regularization schemes, the work distribution itself is well defined and converges as M^{-1} or M^{-2} for the Fourier and the bead regularizations, respectively, in spite of the fact that the average energy $\langle H\rangle$ diverges linearly with M.

C. Convergence of the Jarzynski relation

We will end this section with an explicit demonstration that Jarzynski's nonequilibrium work relation is obeyed and converges to the correct quantum result in the limit $M\to\infty$. First note from Eq. (29) that the left-hand side of Eq. (9) may be reformulated as $\langle\exp(-\beta W)\rangle_{\lambda_A}=G(i\beta)$. Using Eqs. (33), (36), and (37), one finds

$$\langle e^{-\beta W}\rangle = \frac{\omega_A}{\omega_B}\prod_{k=1}^{k_c}\frac{\omega_k^2+\omega_A^2}{\omega_k^2+\omega_B^2}. \tag{52}$$

This product coincides with the product on the right-hand side of Eq. (17), showing that the Jarzynski equality $\langle e^{-\beta W}\rangle = e^{-\beta\Delta F}$ holds and that the resulting free-energy difference converges to the exact result in the limit $M\to\infty$ in the same way, i.e., as $1/M$ for the Fourier regularization and as $1/M^2$ for the bead regularization, as expected from Eqs. (43), (48), and (51).

VI. FINITE SWITCHING SPEED

A. Work distribution

Consider now the case in which the switch from ω_A to ω_B is done in a finite (fictitious) time τ, using the protocol

$$\omega^2(t) = \omega_A^2 + \Delta\omega^2\frac{t}{\tau}, \tag{53}$$

where $\Delta\omega^2$ was defined in Eq. (46), so that $\omega^2(\tau)=\omega_B^2$.

As in the quasistatic process, the Fourier modes are independent and can be handled separately using a time-dependent frequency $\Omega_k(t)$ defined through Eqs. (13) and (53). The solution of Eqs. (31a) and (31b) for a set of initial conditions $\mathbf{X}_k(0)=(\tilde{x}_k(0),\tilde{p}_k(0))$ for this switching protocol can be written as a linear mapping

$$\mathbf{X}_k(t) = \mathsf{M}_k(t)\mathbf{X}_k(0), \tag{54}$$

where $\mathrm{Det}\,\mathsf{M}_k(t)=1$ since the dynamics conserves phase-space volume. The mapping matrix $\mathsf{M}_k(t)$ can be written explicitly in terms of the Airy functions [18] $\phi_1(t)=\mathrm{Ai}[-\Omega_k^2(t)/b]$ and $\phi_2(t)=\mathrm{Bi}[-\Omega_k^2(t)/b]$ with $b=(|\Delta\omega^2|/\tau)^{2/3}$ as

$$\mathsf{M}_k(t) = \tilde{\mathsf{M}}_k(t)\tilde{\mathsf{M}}_k^{-1}(0), \tag{55}$$

where

$$\tilde{\mathsf{M}}_k(t) = \begin{pmatrix} \phi_1(t) & \phi_2(t) \\ m\dot{\phi}_1(t) & m\dot{\phi}_2(t) \end{pmatrix}, \tag{56}$$

which yields

$$\mathsf{M}_k(t) = \pi\begin{pmatrix} \mathrm{Ai}(-y_t)\mathrm{Bi}'(-y_0) - \mathrm{Bi}(-y_t)\mathrm{Ai}'(-y_0) & \frac{\sigma}{m\sqrt{b}}[\mathrm{Ai}(-y_t)\mathrm{Bi}(-y_0) - \mathrm{Bi}(-y_t)\mathrm{Ai}(-y_0)] \\ \sigma m\sqrt{b}[\mathrm{Bi}'(-y_t)\mathrm{Ai}'(-y_0) - \mathrm{Ai}'(-y_t)\mathrm{Bi}'(-y_0)] & \mathrm{Bi}'(-y_t)\mathrm{Ai}(-y_0) - \mathrm{Ai}'(-y_t)\mathrm{Bi}(-y_0) \end{pmatrix}, \tag{57}$$

where $\sigma=\pm 1$ depending on the sign of $\Delta\omega^2$, $y_t=\Omega_k^2(t)/b$, and Ai′ and Bi′ are the derivatives of the Airy functions.

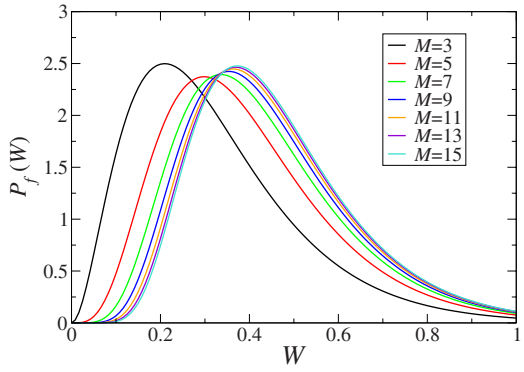

FIG. 3. (Color online) Convergence of the quantum forward work distributions for a quasistatic switching between the potentials in Fig. 1, generated from Eq. (39) using the bead dispersion relation (15). Plotted is $P_f(W)$ for various values of M.

Defining a diagonal matrix

$$\mathsf{D}_k(t) = \begin{pmatrix} \frac{1}{2}m\Omega_k^2(t) & 0 \\ 0 & \frac{1}{2m} \end{pmatrix},$$

the energy contribution of mode k at time t can be written as

$$H_k(t) = \mathbf{X}_k^T(t)\mathsf{D}_k(t)\mathbf{X}_k^T(t) = \mathbf{X}_k^T(0)\mathsf{H}_k(t)\mathbf{X}_k^T(0), \tag{58}$$

where the "Hamiltonian" matrix is given by

$$\mathsf{H}_k(t) = \mathsf{M}^T(t)\mathsf{D}_k(t)\mathsf{M}(t). \tag{59}$$

From Eq. (12), the work contribution of mode k can then be written as

$$W_k = \mathbf{X}_k^T(0)[\mathsf{H}_k(\tau) - \mathsf{D}_k(0)]\mathbf{X}_k(0),$$

where we used that $\mathsf{H}_k(0) = \mathsf{D}_k(0)$. It is now straightforward to compute the generating function $G_k(u)$ of W_k,

$$G_k(u) = \frac{\int d\mathbf{X}_k(0) e^{\mathbf{X}_k^T(0)[iu\mathsf{H}_k(\tau) - (\beta + iu)\mathsf{D}_k(0)]\mathbf{X}_k(0)}}{\int d\mathbf{X}_k(0) e^{-\beta \mathbf{X}_k^T(0)\mathsf{D}_k(0)\mathbf{X}_k(0)}} = \left[\mathrm{Det}\left(\mathsf{I} - \frac{iu}{\beta}\mathsf{C}_k\right)\right]^{-1/2}, \tag{60}$$

where I is the identity matrix and

$$\mathsf{C}_k = \mathsf{D}_k^{-1/2}(0)\mathsf{H}_k(\tau)\mathsf{D}_k^{-1/2}(0) - \mathsf{I}. \tag{61}$$

To illustrate the dependence of the work distributions on τ, we need to perform the Fourier inverse on $G(u) = \Pi_k G_k(u)$. For $|k| > 0$, this is simple, since k and $-k$ are degenerate and yield the combined contribution

$$G_k^2(u) = \frac{1}{\mathrm{Det}\left(\mathsf{I} - \frac{iu}{\beta}\mathsf{C}_k\right)} = \frac{1}{1 - iu\frac{\lambda_k^{(1)}}{\beta}} \frac{1}{1 - iu\frac{\lambda_k^{(2)}}{\beta}}, \tag{62}$$

where $\lambda_k^{(1)}$ and $\lambda_k^{(2)}$ are the two eigenvalues of C_k. The right-hand side of Eq. (62) has the form of two independent exponential modes with rates $\beta/\lambda_k^{(1,2)}$. The Fourier inverse of $\Sigma_{0<|k|\leq k_c} G_k(u)$ is therefore

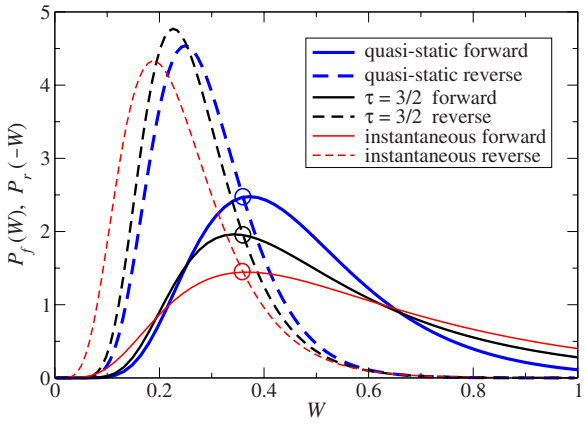

FIG. 4. (Color online) Forward and reverse quantum work distributions for various switching speeds between the harmonic potentials in Fig. 1, generated from Eq. (39) for the quasistatic case, from Eq. (65) for the finite $\tau = 3/2$, and from Eq. (73) for the instantaneous case. Note that the intersection points occur at the same value of W, as they must according to the Crooks fluctuation relation.

$$\tilde{P}(W) = \Theta(\gamma_0' W) \sum_{k=1}^{2k_c} \frac{|\gamma_k'|}{\prod_{\substack{q=1 \\ q\neq k}}^{2k_c} \left(1 - \frac{\gamma_k'}{\gamma_q'}\right)} e^{-\gamma_k' W}, \tag{63}$$

where by definition $\lambda_k^{(i)} = \beta/\gamma'_{2(k-1)+i}$. This expression does not contain the contribution of the mode $k=0$, for which

$$G_0(u) = \frac{1}{\sqrt{\mathrm{Det}\left(\mathsf{I} - \frac{iu}{\beta}\mathsf{C}_0\right)}} = \frac{1}{\sqrt{(1 - iu/\gamma_+)(1 - iu/\gamma_-)}},$$

where $\gamma_+ = \beta/\lambda_0^{(1)}$ and $\gamma_- = \beta/\lambda_0^{(2)}$, and whose Fourier inverse is given by

$$P_0(W) = \sqrt{\gamma_+\gamma_-} e^{-[(\gamma_+ + \gamma_-)/2]W} I_0\left(\frac{\gamma_+ + \gamma_-}{2} W\right), \tag{64}$$

where I_0 is the zeroth-order modified Bessel function of the first kind. The derivation of this result, which holds when γ_+ and γ_- are both positive, is given in Appendix B. In fact it can be shown that for monotonically increasing ω, such as in Eq. (53), γ_+ and γ_- must always be positive, though this restriction need not hold for more complicated protocols.

The complete work distribution function is therefore

$$P(W) = \int_0^W dW' P_0(W')\tilde{P}(W - W'), \tag{65}$$

which unfortunately does not lead to a closed form, but can easily be computed numerically since P_0 and $\tilde{P}$ are known analytically. As an example, the resulting $P(W)$ for the same parameters as for the quasistatic case is shown in Fig. 4 for $\tau = 3/2$, both for the forward and reverse process.

B. Convergence of the work distribution

To determine the convergence properties of the work distribution as $M \to \infty$, we will once again use the cumulants of the work. From the generating function in Eq. (60), we have

$$\sum_{j=1}^{\infty} \frac{(iu)^j}{j!} \kappa_j^{(k)} = -\frac{1}{2} \mathrm{Tr} \ln\left(\mathsf{I} - \frac{iu}{\beta} \mathsf{C}_k\right). \tag{66}$$

By expanding the logarithm and equating like powers of u for $j \geqslant 1$, one finds the cumulants of the different modes to be

$$\kappa_j^{(k)} = \frac{(j-1)!}{2\beta^j} \mathrm{Tr}\, \mathsf{C}_k^j. \tag{67}$$

One thus has for the cumulants of the total work,

$$\kappa_j = \frac{(j-1)!}{2\beta^j} \sum_{|k| \leqslant k_c} \mathrm{Tr}\, \mathsf{C}_k^j.$$

This is of similar form to the expression (44) for the work cumulants in the quasistatic process, which could be shown to converge because of the asymptotic property of γ_k as $k \to \infty$ in Eq. (45). A similar asymptotic property here has to involve the two eigenvalues $\lambda_k^{(1)}$ and $\lambda_k^{(2)}$ of the real symmetric 2×2 matrix C_k for large k. This asymptotic analysis starts with the behavior of the Airy functions for large negative arguments [18]

$$\mathrm{Ai}(-y) \sim \frac{\sin\left(\frac{2}{3} y^{3/2} + \frac{\pi}{4}\right)}{\pi^{1/2} y^{1/4}}, \tag{68a}$$

$$\mathrm{Bi}(-y) \sim \frac{\cos\left(\frac{2}{3} y^{3/2} + \frac{\pi}{4}\right)}{\pi^{1/2} y^{1/4}}, \tag{68b}$$

$$\mathrm{Ai}'(-y) \sim -\frac{\cos\left(\frac{2}{3} y^{3/2} + \frac{\pi}{4}\right)}{\pi^{1/2}} y^{1/4}, \tag{68c}$$

$$\mathrm{Bi}'(-y) \sim \frac{\sin\left(\frac{2}{3} y^{3/2} + \frac{\pi}{4}\right)}{\pi^{1/2}} y^{1/4}, \tag{68d}$$

with corrections of relative $\mathcal{O}(y^{-3/2})$. Using these asymptotic expressions, one can write for the mapping matrix needed in Eq. (61),

$$\mathsf{M}_k(\tau) \sim \begin{pmatrix} \frac{1}{\eta_k} \cos\theta_k & \frac{1}{\eta_k m \Omega_k(0)} \sin\theta_k \\ -\eta_k m \Omega_k(0) \sin\theta_k & \eta_k \cos\theta_k \end{pmatrix}, \tag{69}$$

with $\theta_k = \frac{2}{3}(y_\tau^{3/2} - y_0^{3/2})$ and $\eta_k \equiv \sqrt{\Omega_k(\tau)/\Omega_k(0)}$. Substituting this $\mathsf{M}_k(\tau)$ into Eq. (59) for H_k using $\Omega_k(\tau) = \eta_k^2 \Omega_k(0)$ in $\mathsf{D}_k(\tau)$, and substituting the result into expression (61) for C_k, yields

$$\mathsf{C}_k \sim (\eta_k^2 - 1)\mathsf{I}. \tag{70}$$

Thus it is clear that asymptotically, both eigenvalues of C_k are equal to $\lambda_k^{(1)} = \lambda_k^{(2)} = \eta_k^2 - 1$. But $\eta_k^2 - 1$ is precisely equal to β/γ_k, so that Eq. (67) gives

$$\kappa_j^{(k)} = \frac{(j-1)!}{\beta^j} \left(\frac{\beta}{\gamma_k}\right)^j = \frac{(j-1)!}{\gamma_k^j},$$

which precisely coincides with the asymptotic expression of the cumulants of mode k in the quasistatic case, Eq. (44). In retrospect, this is not too surprising: higher k modes have higher frequencies Ω_k, so that the relative switching speed $1/(\tau\Omega_k)$ decreases for increasing k, resulting in a quasistatic behavior for the work distributions of the high-k modes.

Since the behavior of the work cumulants for large k is the same as in the quasistatic switching, the cumulants themselves converge for the finite-switching speed as well, and in exactly the same way, i.e., $\mathcal{O}(1/M^{2j-1})$ in the Fourier regularization and $\mathcal{O}(1/M^2)$ for the bead regularization. However, it should be stressed that the correspondence between the quasistatic and finite-switching case only holds for the large k modes, and that the lower k modes do differ between the two cases and the total work distribution can vary substantially depending on the switching speed.

C. Convergence of the Jarzynski relation

With these results for the generating function, the Jarzynski equality (9) can be once more checked. Setting $u = i\beta$ in Eq. (60), the generating function gives

$$G_k(i\beta) = \left(\frac{\mathrm{Det}\, \mathsf{D}_k(0)}{\mathrm{Det}\, \mathsf{H}_k(\tau)}\right)^{1/2} = \left(\frac{\mathrm{Det}\, \mathsf{D}_k(0)}{\mathrm{Det}\, \mathsf{D}_k(\tau)}\right)^{1/2} = \frac{\Omega_k(0)}{\Omega_k(\tau)}, \tag{71}$$

where the fact that $\mathrm{Det}\, \mathsf{M}(\tau) = 1$ has been used. Putting together all the contributions to $G(i\beta)$, one obtains the same expression as for the quasistatic case, Eq. (52). The subsequent calculation therefore applies, showing that the Jarzynski relation, Eq. (9), in the form of Eq. (19), also holds for finite-switching rates.

The result in Eq. (19) holds not only for any τ using the protocol in Eq. (53), but in fact for *any protocol*. A different Hamiltonian dynamics would only change the linear mapping $\mathsf{M}_k(\tau)$, which would still obey $\mathrm{Det}\, \mathsf{M}_k(\tau) = 1$, since this follows purely from the Hamiltonian nature of the dynamics. Thus, Eq. (71) would still hold, from which the Jarzynski relation follows.

VII. INSTANTANEOUS SWITCHING

While the work distribution for finite τ could only be expressed analytically up to a convolution, for $\tau = 0$, it is possible to derive a fully analytical form. In this instantaneous limit, the system does not have time to change its positions or momenta, whence $W_k = \frac{1}{2} m \Delta\omega^2 |\tilde{x}_k|^2$. This allows the generating function $G_k(u)$ to be computed, leading to

$$G(u) = \frac{1}{\sqrt{1 - iu\dfrac{\Delta\omega^2}{\beta\omega^2}}} \prod_{k=1}^{k_c} \frac{1}{1 - iu\dfrac{\Delta\omega^2}{\beta\Omega_k^2}}. \quad (72)$$

The generating function can be inverted, to yield

$$\tilde{P}(W) = \Theta(\gamma_0'' W) \sum_{k=1}^{k_c} \frac{|\gamma_k''| \mathrm{erfi}[\sqrt{(\gamma_k'' - \gamma_0'')W}]}{\sqrt{\dfrac{\gamma_k''}{\gamma_0''} - 1} \displaystyle\prod_{\substack{q=1 \\ q\neq k}}^{k_c} \left(1 - \frac{\gamma_k''}{\gamma_q''}\right)} e^{-\gamma_k'' W}, \quad (73)$$

where $\gamma_k'' = \beta\Omega_k^2/\Delta\omega^2$ and $\mathrm{erfi}(x) = -i\,\mathrm{erf}(ix)$ is the complex error function. This work distribution $P(W)$ has also been plotted in Fig. 4, for the same parameters as for the quasistatic and finite-τ cases and both for the forward and reverse process. One sees that regardless of the speed of the process, the crossing points W_c of the forward and reverse distributions are all the same, and equal to the free-energy difference.

To check the convergence of the Jarzynski equality in the instantaneous switching case, one substitutes $u = i\beta$ into Eq. (72). For each of the modes, the generating function at $u = i\beta$ coincides with the result for the finite-switching speed, i.e., the right-hand side of Eq. (71). As a result, the convergence of the free energy as computed from the Jarzynski equality in the instantaneous case is the same as it was for the finite-switching case, as would be expected since the former is the $\tau \to 0$ limit of the latter.

The convergence of the work distribution might be expected to follow similarly by taking the limit $\tau \to 0$ of the cumulants found in the case of finite switching, but it turns out that the limits $\tau \to 0$ and $k \to \infty$ do not commute. The physical reason is that no matter how fast the finite switching is, for fixed positive definite τ and growing k, there are always k modes whose frequencies Ω_k are faster than the switching rate τ^{-1}, and for those modes the switching is nearly quasistatic. But if $\tau = 0$, then the process is instantaneous for all modes, regardless of their k value.

To see the noncommutativity of the limits mathematically, note that for an instantaneous process in which the positions and momenta of the system do not have time to change, the $\mathsf{M}_k(\tau)$ matrix is equal to the identity matrix. The matrix C_k defined in Eq. (61) then assumes the form

$$\mathsf{C}_k = \begin{pmatrix} \dfrac{\Omega_{kB}^2}{\Omega_{kA}^2} - 1 & 0 \\ 0 & 0 \end{pmatrix}, \quad (74)$$

where $\Omega_{kA}^2 = \omega_k^2 + \omega_A^2$ and $\Omega_{kB}^2 = \lim_{\tau\to 0} \Omega_k^2(\tau) = \omega_k^2 + \omega_B^2$. This form is not the same as the $\tau \to 0$ limit of Eq. (70). From Eqs. (67) and (74), one finds for the mode cumulants in the instantaneous switching case

$$\kappa_j^{(k)} = \frac{(j-1)!}{2\beta^j}\left(\frac{\Omega_{kB}^2}{\Omega_{kA}^2} - 1\right)^j = \frac{(j-1)!}{2\gamma_k^j}\left(\frac{\Omega_{kB}}{\Omega_{kA}} + 1\right)^j, \quad (75)$$

where Eq. (37) was used. For large k, $\Omega_{kB}/\Omega_{kA} + 1 \to 2$, so that $\kappa_j^{(k)} \propto \gamma_k^{-j}$ in this regime. Apart from a k independent prefactor, the asymptotic behavior of the cumulants as a function of k is the same as in the previous cases, so that the convergence of the work distribution is also the same.

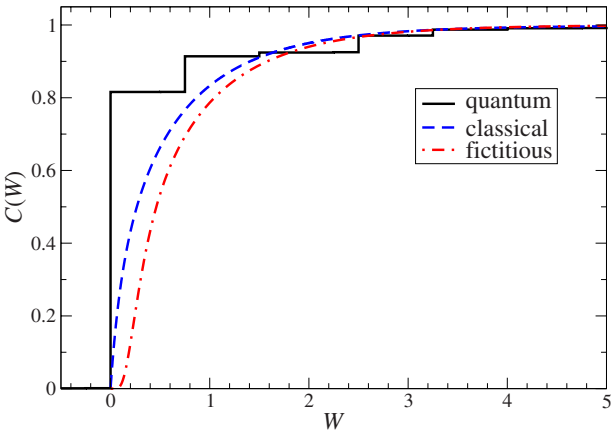

FIG. 5. (Color online) Comparison of the work distributions in the nonequilibrium process of switching the oscillator strength linearly from $\omega_A = 1/2$ to $\omega_B = 5/4$ in a time $\tau = 3/2$, starting in canonical equilibrium with inverse temperature $\beta = 4$, for quantum, classical, and fictitious dynamics.

VIII. COMPARISON WITH REAL TIME QUANTUM DYNAMICS

The viability of the nonequilibrium path-integral approach for the computation of quantum free-energy differences is made possible by the use of a fictitious dynamic, thus avoiding the problems associated with the description of the real time quantum evolution of the system, in contrast to other extensions of the Jarzynski and Crooks fluctuation relations to the realm of quantum mechanics, based on the operator formulation of quantum dynamics [19–25]. As a consequence, however, the work computed within this scheme bears no relation to the work performed in any real quantum process except in the classical limit $\hbar\beta \to 0$, where there are no contributions to the work distribution from the nonzero k modes in the fictitious dynamics. The work distribution for an isolated quantum system in which the frequency is changed in real (rather than fictitious) time has recently been worked out by Deffner and Lutz [25], so that a direct comparison between the fictitious dynamics and real quantum dynamics is possible.

The work distribution for the quantum harmonic oscillator consists of a sum of delta functions, since the real quantum work distribution can be obtained by summing over all possible transitions with the appropriate transition amplitudes worked out by Husimi [26]. Thus, for the purpose of comparison, it is better to consider the cumulative distribution function (CDF) $C(W) = \int_{-\infty}^{W} dw P(w)$ [27]. Figure 5 shows the comparison between the classical CDF [cf. Eq. (64)], the quantum CDF (using Husimi's transition amplitudes), and the CDF resulting from the fictitious path dynamics [cf. Eqs. (63)–(65)] for $\omega_A = 1/2$, $\omega_B = 5/4$, $\tau = 3/2$, and $\beta = 4$. The three curves are obviously very different. The quantum distribution is composed of steps, while the other two are continuous. The quantum distribution also does not agree with

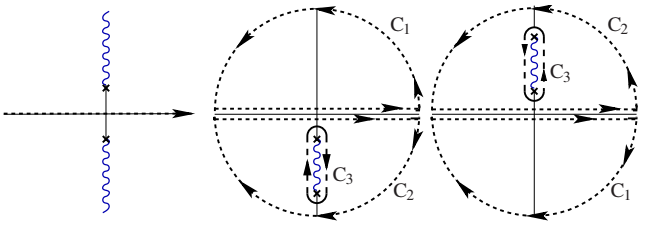

FIG. 6. (Color online) Integration contours (dotted lines) and branch cuts of $G_0(u)$ (wiggly lines) for different signs of γ_+ and γ_-, for the three cases that need to be distinguished in the evaluation of the Fourier inverse in the appendix. The crosses are the singular branch points.

the fictitious dynamics on average. Interestingly, the deviation of the real quantum dynamics from the classical case is less than the deviation from the fictitious dynamics. Another difference between the real quantum dynamics and the dynamics in the other cases is the nonzero probability of negative work values predicted by the distribution, which, as suggested in Ref. [25], is due to excited states decaying to lower states. This negative tail disappears in the classical limit for the monotonic protocol in Eq. (53). The negative tails in the classical limit found in Ref. [25] can only exist for nonmonotonic protocols. Given these observations, it is clear that the fictitious dynamics is very different from real quantum dynamics and has little direct physical content.

IX. CONCLUSIONS

The nonequilibrium methods for the calculation of free-energy differences in quantum systems in the context of the path-integral representation of the canonical partition function presented in the previous paper were applied to the harmonic oscillator to show that the work distribution function is well defined as the regularization parameter M is taken to infinity. Instead of using the real quantum dynamics of the system, the path-integral representation allows a fictitious path to be defined for which the Jarzynski and Crooks relations are valid. By evolving the ring polymer in the path-integral representation under fictitious dynamics, the difficulties associated with the complexity of the full evolution of a quantum system are avoided.

In particular, expressions for the distribution $P(W)$ of the work W done in the nonequilibrium fictitious process in which the strength changes linearly during a time τ, were derived, in the form of a single convolution for finite τ, and in fully explicit form for $\tau \to 0$ (the instantaneous limit) and $\tau \to \infty$ (the quasistatic limit). From $P(W)$, it was shown that the Jarzynski relation holds for this case for any dynamic switching process based on (isolated) Hamiltonian dynamics. The convergence of the resulting free-energy difference was obtained for both regularizations, and goes as $\mathcal{O}(M^{-1})$ for the Fourier regularization and as $\mathcal{O}(M^{-2})$ for the bead regularization. The nature of the convergence of the cumulants of $P(W)$ as $M \to \infty$ was also determined for any τ. Whereas the beads regularization leads to cumulants which all converge as M^{-2}, the jth cumulant converges as $\mathcal{O}(M^{1-2j})$ in the Fourier representation, implying that the shape of the distribution converges faster than its position along the W axis. However, one can use perturbative arguments with the harmonic oscillator as the zeroth-order system to show that the work distributions in the Fourier and bead regularization converge as $1/M$ and $1/M^2$, respectively. Indeed, in the path-integral simulations using the bead regularization presented in the preceding paper [1], one sees a $1/M^2$ convergence for the free-energy difference as well as for the first and second cumulant of the work distribution function. Given the analytical proof given in this paper and the numerical evidence in the preceding paper, it can be expected that the convergence of the method is general.

Other regularization schemes based on the splitting method were also briefly considered and it was found that splitting schemes optimized for molecular dynamics need not be optimal for the convergence of path integrals, in contrast to higher-order splitting schemes which will have better asymptotic convergence properties.

The difference between the fictitious dynamics and real quantum dynamics was demonstrated by direct comparison of the work distribution. Not only is the nature of the distribution different (delta peaks for the quantum case, a smooth function for the fictitious dynamics), but the two also do not agree on average. Nonetheless, the free energy found from the nonequilibrium method with fictitious dynamics is the exact quantum free-energy difference.

ACKNOWLEDGMENTS

We would like to thank Sebastian Deffner for helpful correspondence. The authors would like to acknowledge support by grants from the Natural Sciences and Engineering Research Council of Canada (NSERC). Acknowledgment is made by R.v.Z and J.S. to the Donors of the American Chemical Society Petroleum Research Fund for partial support of this research. L.H.d.l.P. also acknowledges support from the National Science Foundation under Grant No. CHE 04-27082 ITR.

APPENDIX A: ENERGY CONSERVATION OF THE CLASSICAL HARMONIC OSCILLATOR UNDER THE HOA2 INTEGRATION SCHEME

The HOA2 scheme is a second-order integrator for molecular dynamics simulations, like the Verlet scheme, but contains a parameter η which can be tuned to make the dynamics as accurate as possible [13,14,28]. In this appendix, the level of energy conservation as a function of η will be determined explicitly for the classical harmonic oscillator.

The state of the classical harmonic oscillator is represented by a position x and momentum p. Combining these quantities into a two-dimensional vector $\Gamma=(\omega x, p/m)$, the energy of the oscillator is given by $E=\frac{m}{2}|\Gamma|^2$.

In applying the HOA2 splitting scheme in Eq. (23) to molecular dynamics, the kinetic operator $\hat{T}$ is to be replaced by the free Liouville operator $\mathcal{L}_T=\{p^2/2m, \}$ and the potential operator $\hat{V}$ by the interaction Liouville operator

$\mathcal{L}_V=\{V(r),\ \}$, where $\{\ ,\ \}$ is the Poisson bracket operator. The sum of these two Liouville operators is the full Liouvillian $\mathcal{L}=\mathcal{L}_T+\mathcal{L}_V$. Because of the linearity of the equations of motion of the classical harmonics oscillator, the exponentials of these two Liouville operators can be written as the matrices

$$e^{\mathcal{L}_T t}=\mathsf{A}(t)=\begin{pmatrix}1 & \tau\\ 0 & 1\end{pmatrix}, \tag{A1}$$

$$e^{\mathcal{L}_V t}=\mathsf{B}(t)=\begin{pmatrix}1 & 0\\ -\tau & 1\end{pmatrix}, \tag{A2}$$

respectively, which act on the vector Γ, and where $\tau=\omega t$. For the one-step propagator, one thus finds from Eq. (23),

$$e^{\mathcal{L}t/M}\approx \mathsf{B}\left(\frac{\eta t}{M}\right)\mathsf{A}\left(\frac{t}{2M}\right)\mathsf{B}\left(\frac{(1-2\eta)t}{M}\right)\mathsf{A}\left(\frac{t}{2M}\right)\mathsf{B}\left(\frac{\eta t}{M}\right)=\begin{pmatrix}1-\dfrac{\tau^2}{2M^2}+\dfrac{\eta(1-2\eta)\tau^4}{4M^4} & \dfrac{\tau}{M}-\dfrac{(1-2\eta)\tau^3}{4M^3}\\ -\dfrac{\tau}{M}+\dfrac{\eta(1-\eta)\tau^3}{M^3}-\dfrac{\eta^2(1-2\eta)\tau^5}{4M^5} & 1-\dfrac{\tau^2}{2M^2}+\dfrac{\eta(1-2\eta)\tau^4}{4M^4}\end{pmatrix}. \tag{A3}$$

We will denote this approximate propagator matrix by $\mathsf{P}(t/M)$. The approximate propagator $\mathsf{P}(t)$ over a time t is given by the Mth power of $\mathsf{P}(t/M)$, which can be evaluated by diagonalization as follows:

$$\mathsf{P}\left(\frac{t}{M}\right)=\mathsf{U}\ \mathrm{diag}(\mu_1,\mu_2)\mathsf{U}^{-1}, \tag{A4}$$

with μ_1 and μ_2 the eigenvalues of $\mathsf{P}(t/M)$, so that

$$\mathsf{P}(t)=\mathsf{U}\ \mathrm{diag}(\mu_1^M,\mu_2^M)\mathsf{U}^{-1}. \tag{A5}$$

Because we want to minimize the error in front of the leading correction term, we only need the expansions of the eigenvalues and of U in inverse powers of M. The eigenvalues may be expressed as

$$\mu_1=1+\frac{i\tau}{M}-\frac{\tau^2}{2M^2}-\frac{i(1+2\eta-4\eta^2)\tau^3}{8M^3}+\mathcal{O}\left(\frac{1}{M^4}\right),$$

$$\mu_2=1-\frac{i\tau}{M}-\frac{\tau^2}{2M^2}+\frac{i(1+2\eta-4\eta^2)\tau^3}{8M^3}+\mathcal{O}\left(\frac{1}{M^4}\right),$$

whence

$$\mu_1^M=e^{i\tau}\left[1+\frac{i(1-6\eta+12\eta^2)\tau^3}{M^2}+\mathcal{O}\left(\frac{1}{M^3}\right)\right],$$

$$\mu_2^M=e^{-i\tau}\left[1-\frac{i(1-6\eta+12\eta^2)\tau^3}{M^2}+\mathcal{O}\left(\frac{1}{M^3}\right)\right],$$

while the matrix U can be written as

$$\mathsf{U}=\begin{pmatrix}-i+\dfrac{i(1-6\eta+4\eta^2)\tau^2}{8M^2} & i-\dfrac{i(1-6\eta+4\eta^2)\tau^2}{8M^2}\\ 1 & 1\end{pmatrix}+\mathcal{O}\left(\frac{1}{M^3}\right).$$

Substituting these expressions into Eq. (A5), the deviations in the total energy from its initial value as a function of the initial conditions x_0 and p_0 can be written as

$$\begin{aligned}E(t)-E(0)&=\frac{1}{2}m|\mathsf{P}(t)\Gamma_0|^2-\frac{1}{2}m|\Gamma_0|^2\\&=\frac{(1-6\eta+4\eta^2)\tau^2\sin^2\tau}{8M^2}(m\omega^2x_0^2-p_0^2/m\\&\quad-2\omega x_0p_0\cot\tau)+\mathcal{O}(M^{-4}).\end{aligned} \tag{A6}$$

Thus, the leading violation of energy conservation is of order $1/M^2$ for general η. In particular, the Verlet scheme, for which $\eta=1/4$, has second-order violations in the energy conservation. Equation (A6) shows that the leading order violation can be eliminated altogether by taking the solution of $1-6\eta+4\eta^2=0$, i.e., $\eta=(3\pm\sqrt{5})/4$. The larger of these solutions leads to negative time steps in the HOA2 scheme, which can lead to instabilities, so the value of η to take is $\eta=(3-\sqrt{5})/4=0.190\ 983\ 005\ 625\ 052\ 6\ldots$. This value of η makes the scheme pseudo-fourth-order for the harmonic oscillator, and is very close to the general optimized value of $\eta=0.193\ 183\ 327\ 503\ 783\ 6\ldots$ [28], which has been demonstrated to have smaller variations in the total energy than the Verlet scheme for general potentials in numerical simulations [15].

APPENDIX B: FOURIER INVERSE FOR THE CLASSICAL WORK DISTRIBUTION

To arrive at the classical result Eq. (64) for the finite-τ switching process, one needs to compute

$$P_0(W) = \frac{1}{2\pi}\int_{-\infty}^{\infty} du \frac{e^{-iuW}}{\sqrt{(1-iu/\gamma_+)(1-iu/\gamma_-)}}. \quad \text{(B1)}$$

The integrand is a two-valued complex function with two singularities $-i\gamma_\pm$, which are also the branch points. The branch to take in the integral should be that for which the integrand is 1 at $u=0$ [since $G_0(0)=\int dW P_0(W)=1$]. In addition, no branch cut should be crossed as one integrates from $-\infty$ to $+\infty$, i.e., the branch cut should not cross the real axis. This restricts the choice of where to put the branch cut: if γ_+ and γ_- are of opposite sign, with $\gamma_+>0$ say, then in order to avoid a branch cut on the real axis the branch cut should have two parts, one extending from $-i\gamma_+$ to $-i\infty$ and one from $i|\gamma_-|$ to $i\infty$, as in the left panel of Fig. 6. If, on the other hand, γ_+ and γ_- are both positive, then the branch points $-i\gamma_\pm$ both lie on the negative imaginary axis, and it is convenient to put the branch cut between the two branch points, as indicated in the middle panel of Fig. 6, while if γ_+ and γ_- are both negative, the situation is mirrored with respect to the real axis, as shown in the right panel of Fig. 6. This third case can also be treated by setting $W\to -W$ and $u\to -u$ in Eq. (B1), and therefore does not need to be treated separately.

For the first case, i.e., γ_+ and γ_- of opposite sign, with γ_- chosen negative, one can shift the integration line up or down without hitting the branch points, until the integration line passes straight through the middle of the two branch points. In the integral in Eq. (B1), this corresponds to a shift of the integration variable over $i(\gamma_++\gamma_-)/2$. Performing in addition a scaling, such that $u=[-i(\gamma_++\gamma_-)+t|\gamma_+-\gamma_-|]/2$, gives

$$P_0(W) = \frac{\sqrt{\gamma_+|\gamma_-|}}{2\pi} e^{-[(\gamma_++\gamma_-)/2]W}\int_{-\infty}^{\infty} dt \frac{e^{-[(i|\gamma_+-\gamma_-|)/2]Wt}}{\sqrt{1+t^2}}$$
$$= \frac{\sqrt{\gamma_+|\gamma_-|}}{\pi} e^{-[(\gamma_++\gamma_-)/2]W} K_0\left(\frac{|(\gamma_+-\gamma_-)W|}{2}\right), \quad \text{(B2)}$$

using formula 8.432.5 in Gradshteyn and Ryzhik with $\nu=0$ and $z=1$ [29]. This result was also found by Deffner and Lutz [Eq. (27) in Ref. [25]] when they considered the classical limit of a real quantum dynamical process. However, γ_+ and γ_- can only have opposite signs if the oscillator frequency is changed nonmonotonically, which is not the case considered in the text.

If γ_+ and γ_- are both positive, which occurs for monotonically increasing oscillator frequencies [cf. Eq. (53)], one cannot simply shift the integration line to run in between the branch points since one of the branch points would be crossed. The integral is then evaluated as follows. For $W<0$, one can construct a contour C_1 composed of the real axis and an infinite semicircle in the upper half of the complex plane, as shown in Fig. 6. Because for $W<0$, the factor e^{-iuW} decays exponentially when u has a large positive imaginary component, the semicircle does not contribute to the integral, and the contour integral over C_1 has the same value as the original integral. Since no singularities lie within this contour, the integral is zero, proving that for $W<0$, the integral is zero. If, on the other hand, W is positive, then the integrand decays for u with a large negative imaginary component, and the integral can be replaced by an integration over the closed contour C_2 found by adding an infinite semicircle in the lower half of the complex plane, cf. Fig 6. Note that because of the location of the branch cut, one remains on the same branch of the function going along C_2, which is a requirement for the contour to be truly closed. The contour C_2 does contain singularities, and in particular, it contains the branch cut. The contour can be deformed without crossing singularities to the contour C_3 in Fig. 6 which goes around the branch cut. One easily shows that the contributions from the parts that go around the branch points vanish. Furthermore, the integrand changes sign across the branch cut and the contour is traversed in opposite directions on either side, so that the contributions from the left and the right segments of C_3 are equal, and the integral becomes

$$P_0(W) = \int_{-i\gamma_+}^{-i\gamma_-} du \frac{e^{-iuW}}{\pi\sqrt{(1-iu/\gamma_+)(1-iu/\gamma_-)}}. \quad \text{(B3)}$$

Changing integration variables to t, where $u=[-i(\gamma_++\gamma_-)+it(\gamma_+-\gamma_-)]/2$ reduces this integral to

$$P_0(W) = \frac{\sqrt{\gamma_+\gamma_-}}{\pi} e^{-[(\gamma_++\gamma_-)/2]W}\int_{-1}^{1} dt \frac{e^{-[(\gamma_+-\gamma_-)/2]Wt}}{\sqrt{1-t^2}}. \quad \text{(B4)}$$

Given the representation of the modified Bessel function of the first kind given by formula 8.431.1 in Gradshteyn and Ryzhik with $\nu=0$ [29], one finds Eq. (64).

[1] R. van Zon, L. Hernández de la Peña, G. H. Peslherbe, and J. Schofield, preceding paper, Phys. Rev. E **78**, 041103 (2008).
[2] C. Jarzynski, Phys. Rev. Lett. **78**, 2690 (1997).
[3] C. Jarzynski, Phys. Rev. E **56**, 5018 (1997).
[4] G. E. Crooks, J. Stat. Phys. **90**, 1481 (1998).
[5] G. E. Crooks, Phys. Rev. E **60**, 2721 (1999).
[6] R. P. Feynman and A. R. Hibbs, *Quantum Mechanics and Path Integrals* (MacGraw-Hill, New York, 1965).
[7] R. P. Feynman, *Statistical Mechanics: A Set of Lectures* (Addison-Wesley, Reading, MA, 1972).
[8] B. J. Berne, J. Stat. Phys. **43**, 911 (1986).
[9] B. J. Berne and D. Thirumalai, Annu. Rev. Phys. Chem. **37**, 406 (1986).
[10] H. Carslaw, Math. Gaz. **15**, 71 (1930).
[11] Å. Larson and F. Ravndal, Am. J. Phys. **56**, 1129 (1988).
[12] D. Frenkel and B. Smit, *Understanding Molecular Simulation* (Academic Press, San Diego, 1996).
[13] I. P. Omelyan, I. M. Mryglod, and R. Folk, Comput. Phys. Commun. **151**, 272 (2003).
[14] I. P. Omelyan, I. M. Mryglod, and R. Folk, Comput. Phys. Commun. **146**, 188 (2002).
[15] R. van Zon, I. P. Omelyan, and J. Schofield, J. Chem. Phys.

128, 136102 (2008).
[16] H. Goldstein, *Classical Mechanics* (Addison-Wesley, Reading, Massachusetts, 1980).
[17] R. van Zon and J. Schofield (unpublished).
[18] M. Abramowitz and I. A. Stegun, *Handbook of Mathematical Functions with Formulas, Graphs and Mathematical Tables* (Dover, New York, 1965).
[19] S. Mukamel, Phys. Rev. Lett. **90**, 170604 (2003).
[20] M. Esposito and S. Mukamel, Phys. Rev. E **73**, 046129 (2006).
[21] W. De Roeck and C. Maes, Phys. Rev. E **69**, 026115 (2004).
[22] P. Talkner, P. Hänggi, and M. Morillo, Phys. Rev. E **77**, 051131 (2008).
[23] P. Talkner, E. Lutz, and P. Hänggi, Phys. Rev. E **75**, 050102(R) (2007).
[24] P. Talkner and P. Hänggi, J. Phys. A **40**, F569 (2007).
[25] S. Deffner and E. Lutz, Phys. Rev. E **77**, 021128 (2008).
[26] K. Husimi, Prog. Theor. Phys. **9**, 381 (1953).
[27] S. Deffner (private communication).
[28] I. P. Omelyan, I. M. Mryglod, and R. Folk, Phys. Rev. E **65**, 056706 (2002).
[29] I. S. Gradshteyn and I. M. Ryzhik, *Table of Integrals, Series, and Products*, 6th ed. (Academic Press, San Diego, 2000).